RSC Advances

ROYAL SOCIETY OF CHEMISTRY

PAPER

View Article Online
View Journal | View Issue

Cite this: *RSC Adv.*, 2026, **16**, 27707

Citric acid-modulated carbon dots derived from black tea waste for multifunctional food packaging: anti-counterfeiting and UV-protective preservation

Yulu Liu,[a] Jiamin Li,[a] Yizhou Xiao,[b] Yuchi Chen,[a] Yunkai Zhou,[a] Fangmei Zhou,[a] Bingqi Zhu,[a] Wenxiao Jiang,[c] Xing Chen[b] and Guangming Li *[a]

The application of biomass-derived carbon dots (CDs) in smart food packaging is often limited by their low photoluminescence quantum yield. Here, we report a one-pot hydrothermal synthesis of high-performance CDs from black tea waste using citric acid as a multifunctional modulator. FTIR, XPS, zeta potential, and TEM measurements collectively reveal that citric acid enhances photoluminescence primarily through surface passivation, accompanied by the formation of smaller and more uniform carbon cores with a narrower size distribution. This synergistic modulation, dominated by surface passivation, leads to a 25.5-fold quantum yield enhancement from 0.4% to 10.2%, a narrowed emission spectrum with full width at half maximum reduced from 105.59 nm to 64.95 nm, a prolonged fluorescence lifetime from 2.86 ns to 6.93 ns, and improved photostability. Leveraging these optimized properties, the as-prepared CDs are applied in two functional systems for food applications. As a fluorescent ink, they enable covert anti-counterfeiting patterns that are invisible under ambient light but emit bright blue fluorescence under UV excitation. Additionally, a nanocomposite coating incorporating these CDs significantly extends the shelf life of strawberries at room temperature, as evidenced by reduced weight loss, maintained firmness, and preserved soluble solids content over a six-day storage period. This work presents a citric acid-mediated strategy for upcycling agricultural waste into value-added carbon nanomaterials, advancing sustainable and intelligent food packaging technologies.

Received 14th April 2026
Accepted 18th May 2026

DOI: 10.1039/d6ra03143a

rsc.li/rsc-advances

Introduction

Food safety represents a critical and persistent global challenge, necessitating substantial economic investments in food production to address escalating consumption demands.[1] Yet, during storage and transportation, food products are susceptible to quality deterioration induced by environmental stressors, such as ultraviolet (UV) irradiation, which accelerates oxidative degradation and microbial spoilage.[2] Compounding this issue, the prevalence of inadequate anti-counterfeiting features in packaging facilitates the infiltration of fraudulent products into the market, compromising both brand integrity and consumer health.[3] The integration of functional nanomaterials into packaging matrices can modulate the storage microenvironment, which in turn inhibits deterioration pathways and extends shelf-life.[4] In parallel, the incorporation of traceable anti-counterfeiting components enables end-to-end supply-chain visibility, enhancing the dual assurance of food authenticity and safety.[5] Consequently, the development of advanced materials that synergistically combine preservation performance with anti-counterfeiting traceability holds considerable practical significance for the future of sustainable food packaging systems.

Carbon dots (CDs) are a new class of fluorescent carbon nanomaterials with quasi-spherical morphology and diameters typically below 10 nm, first identified by Xu *et al.* in 2004 from the electrophoretic purification of single-walled carbon nanotubes.[6] In 2006, Sun *et al.* pioneered the demonstration that surface passivation of CDs with organic molecules could effectively enhance the quantum yield of CDs, accelerating rapid progress in the field.[7–9] The synthesis of CDs exhibits remarkable precursor versatility, accommodating virtually all carbon-containing compounds as feasible starting materials.[10,11] Compared with conventional carbon sources, biomass-based materials demonstrate superior advantages for CDs fabrication due to their inherent characteristics as sustainable natural resources, including cost efficiency, abundant availability, environmental sustainability, and renewable nature.[12–15] Notably, the conversion of biomass waste into high-performance CDs achieves the benefits of valorizing low-value biomass waste streams while

[a]*School of Medical Technology and Information Engineering, Zhejiang Chinese Medical University, Hangzhou, Zhejiang 310053, P. R. China. E-mail: guangmingli2020@163.com*

[b]*State Key Laboratory of Food Science and Resources, College of Food Science & Technology, Nanchang University, Nanchang, Jiangxi 330047, P. R. China*

[c]*Department of Nutrition and Food Hygiene, School of Public Health, Shenzhen University Medical School, Shenzhen University, Shenzhen 518055, P. R. China*

producing functional nanomaterials, thereby fully conforming to the fundamental principles of green chemistry and circular economy concepts.[16,17] To date, a wide range of biomass waste, including agricultural byproducts,[18,19] fruit wastes[20,21] and vegetable residues,[22] have been successfully employed as sustainable precursors for CDs synthesis. These CDs exhibit remarkable multifunctionality and have demonstrated excellent performance across a variety of applications. Nevertheless, the generally low quantum yields of biomass-derived CDs remain a significant obstacle to their practical implementation, particularly in applications requiring high levels of this key parameter, such as bioimaging and anti-counterfeiting.[23,24]

Tea, as the most widely consumed beverage globally after water, possesses an extensive consumption base worldwide.[25] Based on the degree of fermentation, tea can be classified into several categories, including green tea, white tea, yellow tea, oolong tea, black tea, and dark tea.[26] Among them, black tea and green tea collectively account for 98% of global tea production, with black tea dominating approximately 78% of the global tea market, establishing itself as the predominant tea variety worldwide.[27] With the popularity of tea-derived products such as bottled tea drinks, instant tea powders, tea seed oils, and tea extracts, industrial tea consumption has shown a steady upward trend.[28–31] Consequently, the generation of tea waste during production and processing has increased significantly. Most tea waste is treated through composting, incineration or landfill, and only a small amount is recycled, which not only causes waste of biomass resources, but also poses a risk to the environment due to the caffeine and other components contained in tea grounds.[32] The conversion of tea waste into valuable carbon-based materials presents a promising solution to these problems.[33,34] In recent years, studies have investigated the utilization of tea waste for the synthesis of CDs.[35,36] Nevertheless, the majority of these studies have centered on green tea waste,[37–40] whereas research regarding the preparation of CDs using black tea waste as a raw material remains in its preliminary stages.[41–43] This discrepancy can be attributed to the fact that green tea retains its unfermented state, featuring a high content of low molecular weight, highly reactive, and heteroatom-rich compounds (*e.g.*, polyphenols and vitamins) even after the brewing process.[44] These characteristics make it easier to form CDs with controllable structures and excellent performance during the carbonization process. In contrast, black tea undergoes extensive compositional transformation during fermentation, leading to the formation of polyphenolic compounds such as theaflavins and thearubigins.[45] These polyphenols are larger, more complex molecular structures formed *via* oxidation during processing. Such structural evolution fundamentally diminishes the suitability of black tea as a carbon source in terms of reaction efficiency, end-product performance, and synthetic controllability. Therefore, converting black tea waste into CDs is inherently plagued by drawbacks and challenges.

In this study, black tea waste is pulverized and subjected to hydrothermal treatment with citric acid to synthesize high-performance CDs (BT-CA-CDs, Scheme 1A). Compared to the CDs derived from black tea waste (BT-CDs), the strategic incorporation of citric acid as a multifunctional modulator led to a remarkable 25.5-fold enhancement in photoluminescence (PL) quantum yield (from 0.4% to 10.2%), along with longer fluorescence lifetime and superior photostability. Systematic comparative analysis reveals that citric acid mediates both surface passivation and growth regulation, thereby concurrently optimizing the core structure and surface states of the CDs. Furthermore, we demonstrate the practical applicability of both CDs and CDs/PVA composite solutions as advanced fluorescent inks for food packaging anti-counterfeiting (Scheme 1B). Meanwhile, relying on the ultraviolet-resistant of BT-CA-CDs, we further explored their practical application value in strawberry preservation (Scheme 1C).

Experimental

Materials and reagents

The citric acid and polyvinyl alcohol (PVA-205) were purchased from Shanghai Aladdin Biochemical Technology Co., Ltd. Sodium hydroxide, sodium chloride, urea, arginine, glutaraldehyde solution (25% in water), and melamine were purchased from Beijing InnoChem Science & Technology Co., Ltd, pH buffers were purchased from Wabcan Biotechnology Co., Ltd, hydrochloric acid was purchased from Guangzhou Howei Pharma Tech Co., Ltd, the black tea was purchased from Hangzhou Tea Factory Co., Ltd. All chemical reagents are analytical grade and used without further purification. Strawberries used in the experiments were freshly harvested from a local farm on the day of testing, with no prior chemical treatment or commercial preservation processing.

Instrumentation

The X-ray diffraction (XRD) patterns were measured using Rigaku SmartLab SE X-ray phase diffraction diffractometer, which operated at a voltage of 40 kV and the radiation source was Cu κα (λ = 1.0546 Å). Transmission electron microscopy (TEM) and high-resolution transmission electron microscopy (HRTEM) images were carried out by JEOL JEM-F200 transmission electron microscope. PL spectra were measured using Hitachi F-7000 fluorescence spectrophotometer with an excitation source of a 700 W xenon lamp. X-ray photoelectron spectroscopy (XPS) spectra were measured by Thermo Scientific K-Alpha X-ray photoelectron spectrometer. The ultraviolet-visible (UV-vis) spectra were obtained from TU-1901 UV-vis spectrophotometer. Fourier transform infrared (FT-IR) spectra were measured by Thermo Fisher Scientific Nicolet iS20 FT-IR spectrometer. Zeta potential was measured by Malvern Panalytical Zetasizer Pro zeta potential analyzer. The measurements of absolute PLQY and fluorescence lifetime of all CDs samples were conducted using the FLS1000 PL spectrometer equipped with a QYPro™ integrating sphere. The total soluble solid content of strawberries was tested using Shangyi SN-DR-5310 digital refractometer. The hardness of the strawberries was measured using the Shangyi SN-FH-D004 fruit hardness tester.

Preparation of BT-CDs and BT-CA-CDs

The purchased black tea leaves were brewed repeatedly with boiling water until the brewed water was almost colorless. Then,

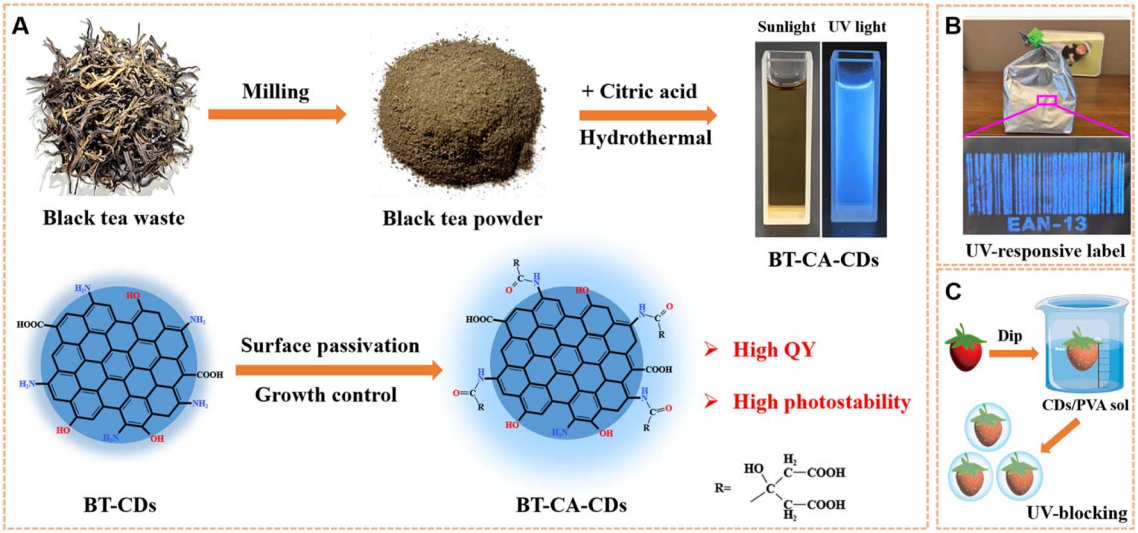

Scheme 1 (A) Schematic of the synthetic route of BT-CA-CDs and PL enhancement mechanism; the application of BT-CA-CDs for fluorescent ink (B) and strawberry preservation (C).

the brewed tea leaves were dried and ground into powder using a grinder. BT-CDs were prepared by mixing tea powder (0.5 g) with pure water (30 mL). For BT-CA-CDs synthesis, black tea powder (0.5 g) and citric acid (0.5 g) were used as co-precursors. These mixtures were placed in Teflon-lined stainless steel and heated at 180 °C for 12 h. After heating, the large particles were extracted and the pH was adjusted to around 7.0. The resulting solution was dialyzed using dialysis bag (500 Da) for 24 h, and then filtered by a membrane (0.22 μm) to obtain the high-quality sample. We also investigated whether urea, arginine, and melamine could improve PL intensity of black tea waste-based CDs. The fluorescence emission results showed that none of them could improve the PL intensity of black tea waste-based CDs as much as citric acid (Fig. S1–S4). Batch-to-batch reproducibility was thoroughly verified by performing three independent syntheses, each of which yielded highly consistent fluorescence spectra after normalization, demonstrating the reliability of this method (Fig. S5).

Calculation of quantum yield

The quantum yield of CDs was measured by using an absolute QY measurement system with an integrating sphere, using the formula:[46]

$$\varphi_{\mathrm{PLQY}} = \frac{\int_{\lambda_3}^{\lambda_4} \left| I_{\text{sample emission}} - I_{\text{reference emission}} \right| \mathrm{d}\lambda}{\int_{\lambda_1}^{\lambda_2} \left| I_{\text{reference scatter}} - I_{\text{sample scatter}} \right| \mathrm{d}\lambda}.$$

Effect of reaction system pH on CDs synthesis

Two sets of starting materials (0.5 g black tea waste powder, 0.5 g black tea powder and 0.5 g citric acid) were prepared. The pH values of sample solutions were adjusted to 1.0, 7.0, and 13.0 using HCl and NaOH solutions prior to hydrothermal treatment. Notably, the initial pH of the black tea waste and citric acid mixture was approximately 1.0 without any adjustment. The pH-adjusted starting materials were then subjected to hydrothermal reaction at 180 °C for 12 h in 50 mL autoclaves. After reaction, the crude products were collected by filtration for testing UV-vis absorption. To obtain final products, the crude products were dialyzed for 24 h and filtered through membranes (0.22 μm) for fluorescence measurements.

Exploring the stability of CDs

The prepared BT-CDs and BT-CA-CDs solutions were diluted to achieve an optical density of 0.10 ± 0.02 at 400 nm. The stability of the samples was then evaluated under various conditions including different pH (1.68–12.48), temperatures (25–75 °C), NaCl concentrations (0–1.0 M), and UV light irradiation (365 nm, 0–120 min).

Preparation of fluorescent inks

The synthesized BT-CA-CDs solution was diluted with pure water at a 1 : 4 ratio until no visible traces were observed on white paper under natural light. This diluted solution could be directly loaded into a standard pen as fluorescent ink, exhibiting smooth writing performance and clearly visible text under 365 nm UV light excitation. To enhance the adhesion of the ink for application *via* stamps, PVA solutions at varying concentrations were tested. Experimental results demonstrated that CDs fluorescent ink containing 4% PVA solution produced the most complete and well-defined stamp patterns. This ink was also applied *via* stamp printing to create EAN-13 barcodes on various food packaging substrates. The pattern integrity and legibility of the printed barcodes were examined under 365 nm ultraviolet excitation. Aluminium foil specimens bearing the printed barcodes were divided into two test groups: one underwent cross-linking treatment with glutaraldehyde (in a sealed system at 80 °C for 12 h), while the control group

remained untreated. Both sample sets were then subjected to water resistance testing. A drop of DI water was placed on the surface of each sample and maintained for 1 min. After removing excess water, the surface morphology and changes of the samples were observed and compared.

Experimental study on the preservation of strawberries using BT-CA-CDs

In the experiment, 90 strawberries of similar maturity and size were selected and randomly divided into three groups of 30 strawberries in each group. The three groups of strawberries were soaked in the corresponding treatment solution for 30 s, among which the blank control group was distilled water, the PVA group was 5% PVA solution, and the PVA + CDs group was a composite solution of 0.01% BT-CA-CDs and 5% PVA. The treated strawberries were stored in a room temperature environment to compensate for natural light exposure, during which changes in surface ripeness were observed and recorded daily for each group. The images of the strawberry appearance were taken on days 0, 2, 4, and 6 of storage. The weight change during strawberry storage was calculated by the weighing method, and its weight loss rate is calculated (weight loss rate calculation formula: weight loss (%) = $[(W_0 - W_1)/W_0] \times 100\%$). Each strawberry was tested for hardness by using a standard probe to penetrate the flesh uniformly at a constant speed, with the maximum force value recorded. The strawberries were squeezed into juice, and the soluble solids content of the juice was determined using a handheld refractometer.

Results

Morphological properties

The TEM images in Fig. 1A and D show that both BT-CDs and BT-CA-CDs are spherical and monodisperse. The average diameters of BT-CDs and BT-CA-CDs are 2.6 ± 0.43 nm and 1.8 ± 0.26 nm (mean $\pm$ SD), respectively, which were calculated from the particle size distribution statistics (Fig. 1C and F). The HRTEM images reveal well-defined lattice fringes in both CDs, with a lattice spacing of 0.21 nm corresponding to the (100) planes of graphitic carbon (Fig. 1B and E). FT-IR is known to be a common technique for characterizing surface functional groups. To determine the types of the CDs surface functional groups, the samples were concentrated and dried to obtain powders for FT-IR spectrometer measurement (Fig. 1G). The FT-IR spectra of black tea waste, BT-CDs and BT-CA-CDs, all of which exhibited some common absorption characteristics. The peak at 3500–3300 cm^{-1} is the overlap of O–H/N–H bond stretching vibrations.[32] The absorption bands at 2993–2831 cm^{-1} correspond to saturated C–H stretching vibrations, while the peak at 1648 cm^{-1} is assigned to the C=O stretching vibration (amide band). The characteristic vibrations of the carboxylate group ($-COO^-$) appear at 1576 cm^{-1} (asymmetric stretching, $\nu_{as}(-COO^-)$) and 1407 cm^{-1} (symmetric stretching, $\nu_s(-COO^-)$). During the hydrothermal reaction, black tea waste undergoes oxidative decomposition to form CDs with abundant surface amino and carboxyl groups. After the introduction of citric acid, the characteristic carboxyl peaks become significantly more pronounced, confirming that citric acid promotes surface carboxyl functionalization. The surface charge properties of the two types of CDs were further investigated by zeta potential measurements as a function of pH. As shown in Fig. S6, both types of CDs exhibited negative surface charges across the tested pH range. Under pH 4 and pH 7, their zeta potentials were very similar, indicating comparable initial surface charge states. As the pH increased from 7 to 10, the negative charge of BT-CDs showed a marked enhancement, with zeta potential shifting from approximately -23.1 mV to -37.8 mV. In contrast, although BT-CA-CDs also became more negatively charged over the same pH range (from approximately -20.8 mV to -29.9 mV), the magnitude of this increase was substantially smaller than that observed for BT-CDs. As a result, the difference in zeta potential between the two CDs gradually widened under alkaline conditions. The results indicate that citric acid modification effectively altered the surface microchemical state of BT-CA-CDs, likely by modulating the content and/or pK_a of surface-dissociable acidic groups, thereby leading to different pH-dependent charge responses of the two types of CDs. Fig. 1H displays a broad diffraction peak centered at $2\theta = 19.83°$ in the XRD patterns of all synthesized CDs, consistent with the typical characteristics of amorphous carbon materials possessing short-range graphitic ordering. Combined with HRTEM analysis, it is proved that as-prepared CDs exist in a microcrystalline state. The d-spacing of 0.45 nm corresponds to the (002) plane of graphite by Bragg equation.[47] The abnormal increase might be caused by steric hindrance of graphene edge functional groups or planar distortion of sp^3 C in the graphene plane. Compared with BT-CDs, the BT-CA-CDs have a smaller particle size and higher surface carboxyl density, which may enhance their dispersibility in water and optical properties.

Compositional analysis

To analyse the chemical composition, XPS spectra of CDs were recorded. The XPS survey spectra of BT-CDs and BT-CA-CDs (Fig. 2A and E) reveal three characteristic binding energy peaks at 284.54/284.37 eV (C 1s), 399.4/399.22 eV (N 1s), and 531.34/530.91 eV (O 1s), confirming the coexistence of carbon, nitrogen, and oxygen as the predominant elemental constituents in both CDs. Quantitative analysis results reveal distinct compositional differences between BT-CDs and BT-CA-CDs. The oxygen content increased from 22.68% to 28.05%, while the carbon content decreased from 69.91% to 65.75%. The increased oxygen content can be reasonably attributed to the inherently high oxygen content of citric acid, which has a theoretical oxygen composition of 58.3% ($C_6H_8O_7$). The C 1s spectra in Fig. 2B and F can be divided into three fitting peaks: 284.35/284.16, 285.80/285.83, and 287.55/287.40 eV, corresponding to C–C/C=C, C–N/C–O, C=O/C=N, respectively.[48] As shown in Fig. 2C and G, the N1s spectra can be classified as pyridine N (399.14 eV/398.91 eV) and pyrrole N (399.81 eV/399.63 eV). The O 1s spectra of BT-CDs (Fig. 2D) and BT-CA-CDs (Fig. 2H) can be deconvoluted into two characteristic fitting peaks. For BT-CDs, the peaks are located at 531.02 eV and 532.34 eV, corresponding to C=O and C–O bonds, respectively. For BT-CA-CDs, the fitted

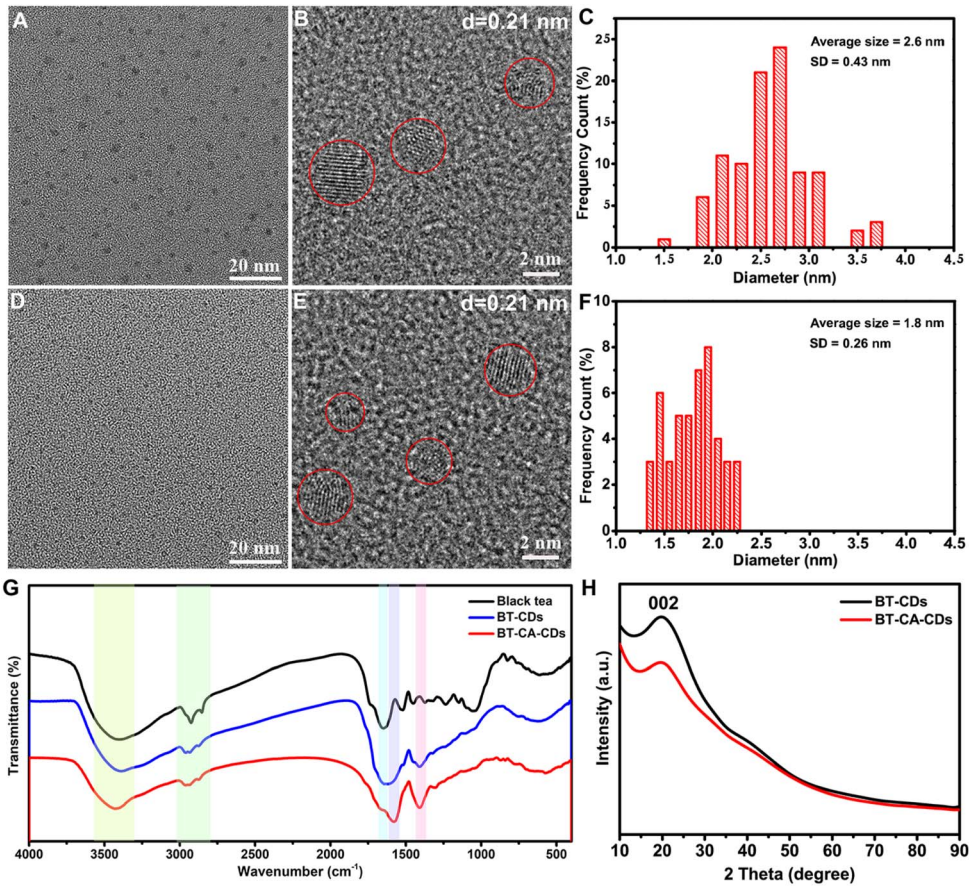

Fig. 1 TEM images of BT-CDs (A) and BT-CA-CDs (D); HRTEM images of BT-CDs (B) and BT-CA-CDs (E); size distribution of BT-CDs (C) and BT-CA-CDs (F); (G) FT-IR spectra of black tea, BT-CDs and BT-CA-CDs; (H) XRD patterns of BT-CDs and BT-CA-CDs.

peaks shift to 530.31 eV (C=O) and 531.16 eV (C–O). XPS results reveal no significant changes in the composition of various chemical bonds, while the introduction of citric acid notably alters the elemental distribution in CDs.

Optical properties

To systematically investigate the optical properties of BT-CDs and BT-CA-CDs, a detailed analysis of their PL spectra was firstly conducted. In the excitation wavelength range of 340–400 nm, the optimal excitation wavelength of both CDs is locked

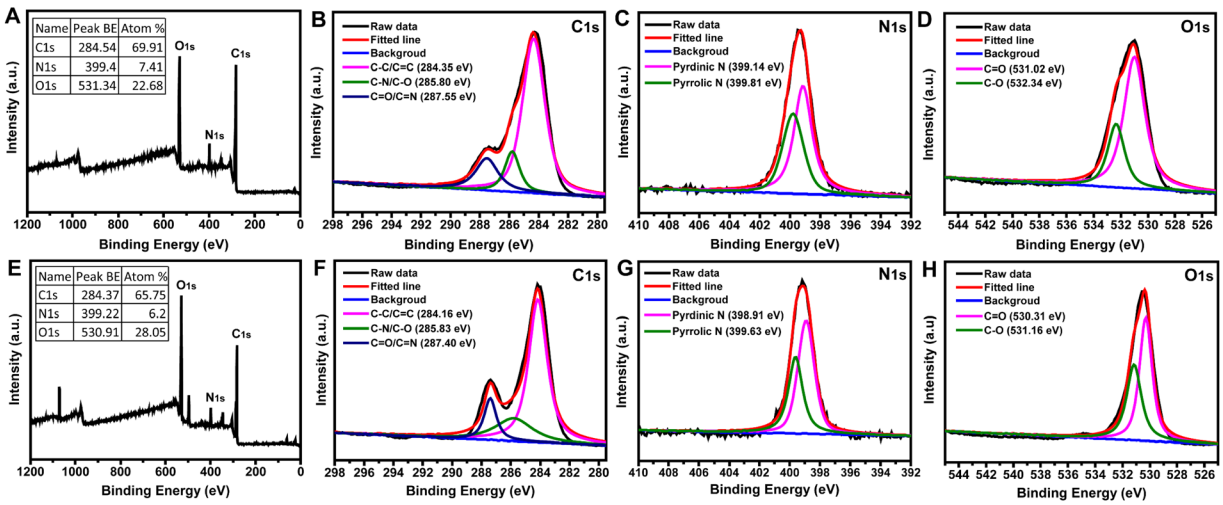

Fig. 2 XPS characterization of BT-CDs and BT-CA-CDs. (A and E) Survey spectra, with insets showing the binding energies and atomic contents of C 1s, N 1s, and O 1s. (B–D) High-resolution C 1s, N 1s, and O 1s spectra of BT-CDs. (F–H) High-resolution C 1s, N 1s, and O 1s spectra of BT-CA-CDs.

at 340 nm. The BT-CDs show a typical excitation-dependent emission: with the gradual increase of excitation wavelength, their fluorescence intensity decrease, and the emission peak has a significant redshift (Fig. 3A). This observation is consistent with the common characteristics of most reported CDs, which can likely be attributed to the conjugated structures formed by aromatic C=C bonds within the CDs and surface defect groups such as hydroxyl (C–OH) and carbonyl (C=O). The BT-CA-CDs exhibit a similar excitation-dependent fluorescent properties, with the optimal emission peak at 409 nm (Fig. 3B). The comparison of the PL spectra under 340 nm excitation reveals a markedly enhanced emission intensity for BT-CA-CDs compared to BT-CDs, exhibiting an approximately 25.5-fold increase, which substantiates their superior fluorescence properties (Fig. 3C). Meanwhile, the BT-CDs exhibit a full width at half maximum of 105.59 nm, while that of the BT-CA-CDs is 64.95 nm, indicating a narrowed emission spectrum. The UV-vis absorption spectra (Fig. 3D) of both CDs exhibit featureless absorption profiles, consistent with CDs prepared by similar methods reported in literature. The absorption edge of BT-CA-CDs shows a blue shift, which may be attributed to their unique surface chemistry or quantum size effects. The fluorescent lifetimes of BT-CDs and BT-CA-CDs were measured under excitation with a 365 nm light source (monitored at 440/415 nm). The PL decay curves are well fitted using the following single-exponential formula: $y = A_1 \exp(-x/t_1) + y_0$. The fluorescence decay times were measured to be 2.86 ns for BT-CDs and 6.93 ns for BT-CA-CDs, with the high quality of the single-exponential fitting validated by a coefficient of determination (R^2) of 0.99. This indicates that they have a nanosecond fluorescent lifetime without phosphorescence or afterglow (Fig. 3E). The longer fluorescence lifetime of BT-CA-CDs compared to that of BT-CDs may be attributed to the enriched surface functional groups after citric acid modification. This enhancement could promote the formation of a more stable rigid structure and/or reduce non-radiative decay pathways caused by surface defects, thereby prolonging the residence time of the excited state. The effect of citric acid dosage on the fluorescent properties of CDs during synthesis was investigated. The addition of citric acid only changed the fluorescence intensity, while the position and shape of the optimal emission peak remained unchanged (Fig. 3F). The above results demonstrate that black tea waste consistently serves as the carbon source throughout the reaction, while citric acid functions as a surface passivation agent, which alters the quantity or distribution of surface groups as well as the elemental content.

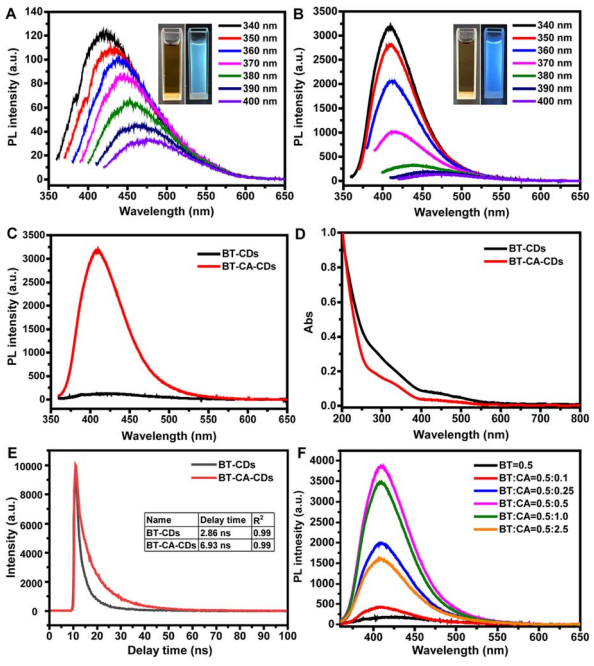

Fig. 3 PL spectra of BT-CDs (A) and BT-CA-CDs (B) at different excitation wavelengths, insets: photographs of BT-CDs and BT-CA-CDs solutions under natural light (left) and 365 nm UV illumination (right); (C) Normalized PL spectra of BT-CDs and BT-CA-CDs under 340 nm excitation; (D) UV-vis absorption spectra of BT-CDs and BT-CA-CDs; (E) fluorescence lifetime decay profiles of BT-CDs and BT-CA-CDs; (F) PL spectra of CDs prepared with different ratios of black tea waste (BT) to citric acid (CA).

Synthesis mechanism

Citric acid, a small molecular acid, can significantly modulates the pH of the reaction system. To investigate whether citric acid plays a role primarily through its acidity during the synthesis of BT-CA-CDs, we adjusted the initial pH (including acidic, neutral, and alkaline conditions) of two stating materials groups (black tea waste only or a mixture of black tea waste and citric acid) prior to the hydrothermal reaction. Subsequently, the optical properties of the resulting reaction solutions and the purified CDs were characterized using UV-Vis absorption spectroscopy and PL spectroscopy. The UV-Vis absorption spectra reveal that both reaction systems display significantly enhanced UV-Vis absorbance under alkaline conditions, correlating with the darkly colored solution depicted at the right of the illustration (Fig. 4A and B). In contrast, the lowest UV-vis absorption was observed under acidic conditions, which is consistent with the light yellow appearance of the solution shown on the left side of the illustration. It indicates that alkaline conditions promote the carbonization of initial starting materials, while acidic conditions play an inhibitory role. According to the PL spectra, the CDs synthesized under acidic conditions exhibit higher PL intensity, with the enhancement being more pronounced in the system where citric acid was introduced (Fig. 4C andD). Given that the average size of BT-CA-CDs (1.8 nm) is smaller than that of BT-CDs (2.6 nm), we speculate that the acidic environment suppresses the growth rate of carbon cores, leading to the formation of carbon cores with fewer internal defects, which in turn influences their light absorption and fluorescence emission behaviours. Further, a control experiment demonstrates that citric acid alone does not exhibit strong fluorescence under identical conditions. (Fig. S7), effectively ruling out the possibility that carbonized citric acid contributes significantly to the observed optical properties. Therefore, it can be concluded that citric acid primarily functions as a multifunctional modulator in the synthesis process,

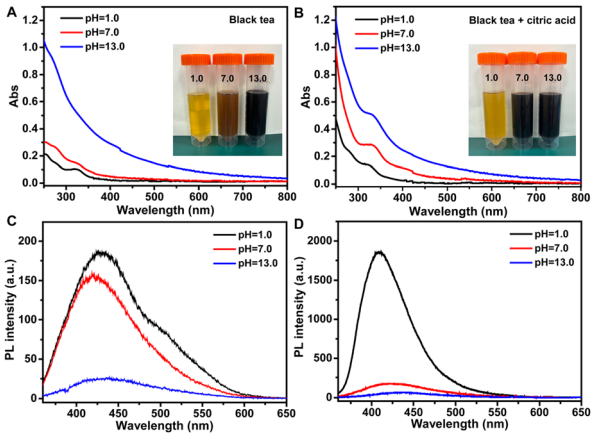

Fig. 4 UV-Vis absorption spectra of crude samples from black tea (A) and black tea + citric acid (B) at pH 1.0, 7.0, and 13.0. Insets: photographs of the crude solutions under natural light. PL spectra (340 nm excitation) of black tea (C) and black tea + citric acid (D) prepared at different pH.

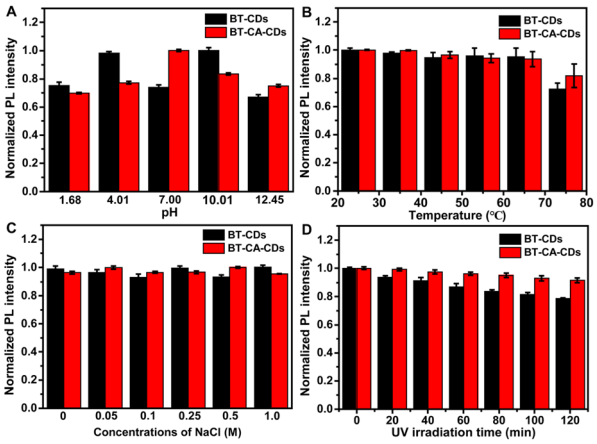

Fig. 5 Effects of pH (A), temperature (B), ionic strength (C), and UV exposure time (D) on the fluorescence intensity of BT-CDs and BT-CA-CDs ($n = 3$).

serving to mitigate both surface and core defects, thereby leading to enhanced PL performance.

PL stability

The effects of pH, temperature, NaCl concentration, and UV exposure time on the PL intensity of BT-CDs and BT-CA-CDs were examined. Two kinds of CDs were mixed into pH buffers (1.68, 4.01, 7.00, 10.01, 12.45) while maintaining consistent OD_{400} absorption. The PL intensity of BT-CDs and BT-CA-CDs exhibit slight fluctuations, showing a moderate reduction under both acidic and alkaline conditions (Fig. 5A). The BT-CDs and BT-CA-CDs exhibit negligible changes in PL intensity between 25–65 °C, while a more pronounced decrease is observed at 75 °C (Fig. 5B). The PL intensity of BT-CDs and BT-CA-CDs remain stable across a NaCl concentration range of 0–1.0 M, indicating that the ionic strength of the solution has a negligible effect on their PL intensity (Fig. 5C). Under 365 nm ultraviolet irradiation, the PL intensity of BT-CDs gradually decreased with increasing exposure time (0–120 min), whereas BT-CA-CDs exhibit markedly higher stability with nearly unchanged intensity (Fig. 5D). This disparity highlights the superior resistance of BT-CA-CDs to UV photodegradation, which may be attributed to their distinct surface states and enhanced chemical bond stability. The stability study demonstrated that BT-CA-CDs exhibit superior thermal and photostability compared to BT-CDs.

Application of BT-CA-CDs as fluorescent ink on paper

Anti-counterfeiting technology plays a critical role in safeguarding commercial transactions, pharmaceutical integrity, and industrial product security. The development of advanced anti-counterfeiting materials that integrate strong fluorescence, facile processability, environmental compatibility, and low cost has emerged as a significant research frontier in materials science. The BT-CA-CDs solution prepared in this study exhibits significant differences in optical properties under natural light and 365 nm ultraviolet light, showing excellent potential for anti-counterfeiting applications. When the BT-CA-CDs solution was used as ink and filled into a standard pen, it could write smoothly on paper. The handwritten contents show clear fluorescence under 365 nm ultraviolet excitation (Fig. 6A–C). As shown in Fig. 6D–G, the flexibility of fluorescent ink in information encryption and anti-counterfeiting identification is further verified through designs such as embedding the number "1953" into the school emblem pattern and hiding "1029" in the number "0323". It is confirmed that the BT-CA-CDs ink can stably write Chinese characters, letters, numbers, as well as complex patterns. However, direct application of BT-CA-CDs ink for stamping proved ineffective in generating complete fluorescent patterns. PVA itself exhibits no fluorescence, and we found the incorporation of 4% PVA markedly enhanced pattern integrity while preserving the intrinsic fluorescence characteristics of the BT-CA-CDs ink (Fig. S8 and S9). Rheological analysis confirm that the viscosity modulation achieved through PVA addition is critical for enabling the reliable formation of well-defined patterns (Fig. S10). As illustrated in Fig. 6H–K, the BT-CA-CDs/PVA ink enable complete stamping of alphanumeric characters, Chinese logograms, and complex patterns. Fig. 6L–O further demonstrate the ink's suitability for producing finely detailed features across varying scales. The written and stamped samples maintain stable fluorescent performance on paper substrates, and can still be clearly identified under ultraviolet excitation after being stored for several months.

Application of BT-CA-CDs on the surface of food packaging

The application of BT-CA-CDs was further extended to food packaging systems. Conventional packaging materials were employed as substrates, which included glass containers, plastic packaging, metal cans, and aluminium foil, as illustrated in Fig. 7A–D. As clearly depicted in Fig. 7E–H, the fluorescent ink we developed could form well-defined EAN-13

Fig. 6 (A–C) Depict samples handwritten on paper with a pen under UV light; (D–G) present a comparative display of numerals under natural light (left) and UV light (right); (H–K) exhibit photos of letters, numerals, Chinese characters, and intricate patterns made by stamps sequentially under UV light; (L–O) show images of the patterns fabricated using stamps of varying sizes, captured under UV light illumination.

traceability barcodes on these materials. To enhance practical applicability, cross-linking treatment with glutaraldehyde was employed to effectively mitigate water penetration and interaction. Comparative tests revealed that the barcode patterns on cross-linked surfaces remained largely intact after mild aqueous treatment, whereas those on non-cross-linked surfaces suffered significant degradation (Fig. 7I–L). These results confirm that glutaraldehyde cross-linking significantly improves the water resistance of patterns fabricated from BT-CA-CDs solution. Clearly, the BT-CA-CDs demonstrate uniform adhesion on diverse food packaging materials, forming clearly identifiable fluorescent barcodes under UV illumination with enhanced water durability. This functionality enables product identification, traceability tracking, inventory management, and price settlement, while providing anti-counterfeiting capabilities—

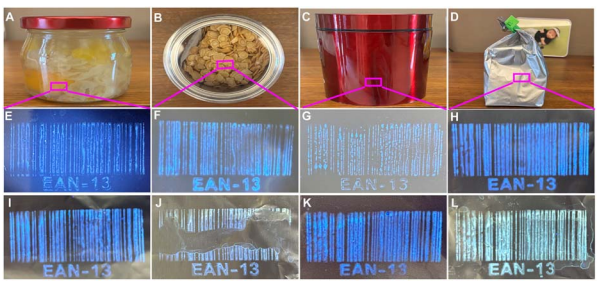

Fig. 7 (A–D) show schematic diagrams of glass containers, plastic packaging, metal cans, and aluminum foil packaging, respectively; fluorescent barcodes on substrates under 365 nm UV: (E) glass, (F) plastic, (G) painted metal, (H) Al foil; fluorescence images of barcodes from the non-crosslinked (I–J) and glutaraldehyde-crosslinked (K–L) groups before and after water resistance testing.

thereby offering robust support for ensuring food safety and supply chain transparency.

Application of BT-CA-CDs in strawberry preservation

During the processing, storage, and retail display of food products, exposure to UV radiation represents a critical factor responsible for quality degradation, reduction in shelf life, loss of nutritional components, and potential safety hazards. The development and application of UV-blocking packaging materials have thus gained considerable attention as an effective approach to mitigate these adverse effects. BT-CA-CDs significantly enhanced the UV-shielding properties of PVA-based packaging materials, owing to their notable UV absorption capacity (Fig. S11). Based on this, three controlled experiments were designed to explore the role and mechanism of BT-CA-CDs in strawberry preservation. Fig. 8A shows the appearance of strawberries in the control group, PVA group, and PVA + CDs group on the day 0, day 2, day 4, and day 6 of storage. It can be seen from the photographs that the three colour, ripeness, leaf water loss degree and decay: the leaves of the control group showed obvious water loss and wilting on the second day of storage; the leaves of PVA group began to shrink on the day 4. The PVA + CDs group maintained good hydration status until the day 5. The degree of water loss in strawberry leaves is closely related to plant respiration transpiration, which suggests that the addition of BT-CA-CDs may enhance the water retention capacity of PVA, thereby inhibiting leaf water loss. In addition, after storage until the day 6, decay and colony growth occurred in both groups (control group and PVA group) without CDs, while this was not the case in the PVA + CDs group, suggesting that BT-CA-CDs may have an inhibitory effect on the growth of microorganisms on the surface of strawberries. Fig. 8B shows the weight change trend of strawberries during storage in each group. Weighing statistics shows that the weight of strawberries in all groups decreased with the prolongation of storage time, and the weight loss of the control group is the most significant (reaching 27.7% on day 6), followed by the PVA group (18.3%), while the PVA + CDs group exhibited the lowest weight loss of only 16.7%. This is consistent with the water loss of leaves in Fig. 8A, which further confirms that the control group had the worst preservation effect and the PVA + CDs group was most effective in inhibiting water loss. The change of strawberry hardness is shown in Fig. 8C. After 6 days of storage, the hardness of the control group dropped sharply to 0.8 kgf cm^{-2}, while the PVA group maintained a hardness of 0.93 kgf cm^{-2}, and the PVA + CDs group retained the highest hardness of 0.94 kgf cm^{-2}. The smallest hardness loss in the PVA + CDs group indicates that the treatment in this group could maintain the hardness of strawberry fruits more effectively and delay the fruit softening process. The total soluble solids content is an important index for evaluating the nutritional value and sweet flavour of strawberries, and the changes in the total sugar content of the three groups of samples during 6 days of storage are shown in Fig. 8D. In the early stage of storage, the total soluble solids content of strawberries in each group increased slightly due to the water loss caused by transpiration. In the

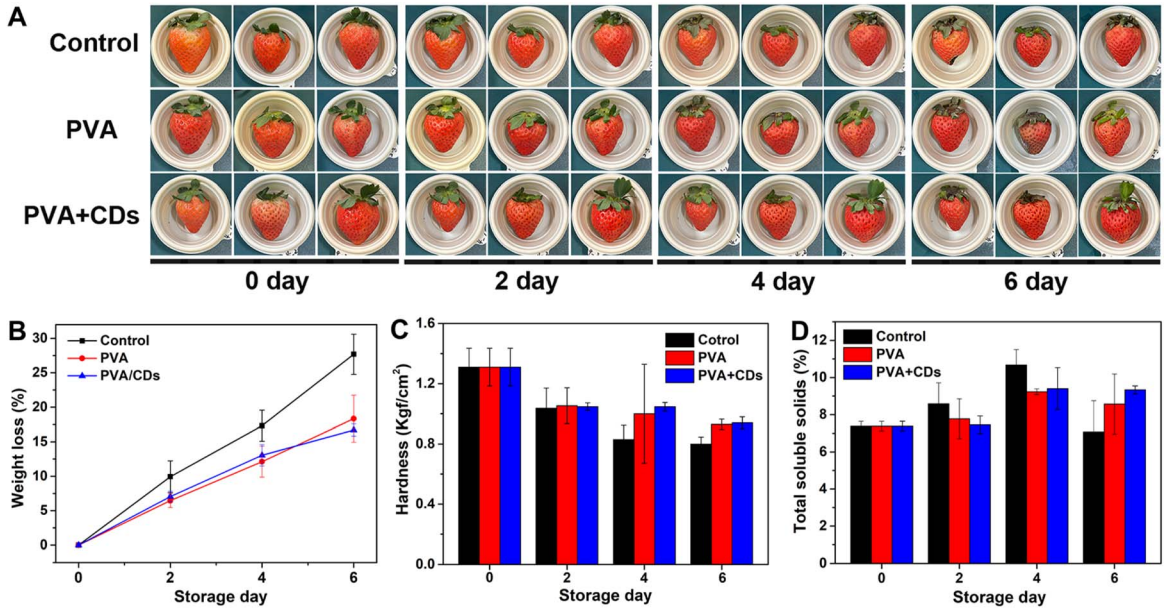

Fig. 8 Effects of different treatments on strawberry quality during 6 days of storage. (A) Representative photographs showing appearance changes of strawberries treated with water (control), PVA solution, and PVA + CDs composite solution. (B) Weight loss, (C) firmness, and (D) total soluble solids (TSS) content over the storage period ($n = 3$).

later stage of storage, the total soluble solids content decreased significantly due to the large number of spoilage microorganisms in the control group and PVA group, and total soluble solids was metabolized and consumed by microorganisms. Specifically, the control group's total soluble solids content fell to 7.0% on day 6, the PVA group to 8.6%, whereas the PVA + CDs group maintained a significantly higher level of 9.3%. By the day 8, strawberries in the control and PVA-only groups showed evident decay, browning, and shriveling, whereas those in the PVA + CDs group remained fresh with green calyxes, bright color, and no signs of decay (Fig. S12). Collectively, by incorporating BT-CA-CDs, the PVA + CDs coating effectively extended the shelf life of strawberries through multiple synergistic mechanisms: it reduced photodegradation *via* UV-blocking, minimized moisture loss by improving the water vapor barrier, and suppressed microbial growth through antibacterial activities. These combined effects resulted in a better preservation performance compared to the control groups. We have compared our work with existing packaging or coating systems reported in recent literature that utilize CDs for strawberry preservation. As summarized in Table S1, representative studies have demonstrated that CDs-based coatings exhibit multiple preservation effects, including reduced decay rate, improved moisture retention, and extended shelf life under different conditions. Compared with these reported systems, our PVA + BT-CA-CDs coating achieves competitive or superior performance after more than 6 days of storage at room temperature, as evidenced by 0% decay rate, low weight loss, and high firmness retention. This comparison places our work within the context of recent advances and confirms that our coating system is an effective strategy for strawberry preservation.

Discussion

In this work, citric acid plays a dual role in defect passivation and growth regulation to tune the properties of CDs derived from black tea waste, with surface defect passivation as the dominant mechanism. The successful incorporation of carboxyl groups was confirmed by FTIR, XPS, and zeta potential measurements. As a result, the optimized CDs exhibit 25.5-fold enhancement in quantum yield from 0.4% to 10.2%, a prolonged fluorescence lifetime from 2.86 ns to 6.93 ns, a narrowed full width at half maximum from 105.59 nm to 64.95 nm, and a reduced average particle size from 2.6 nm to 1.8 nm. Given that pH adjustment alone does not improve fluorescence performance, it can be concluded that the enhanced properties arise from the synergy between carboxyl passivation and the acidic environment, wherein surface passivation is the key factor. The one-step hydrothermal method demonstrated simplicity, cost-effectiveness, and excellent batch-to-batch reproducibility, making it a reliable laboratory-scale synthesis route. For strawberry preservation, the CDs/PVA coating extended shelf life through synergistic mechanisms including UV blocking, moisture regulation, as well as potential antibacterial and antioxidant activities that may originate from tea-derived components retained during the hydrothermal process. Regarding food-contact suitability, CDs derived from natural precursors exhibit good biocompatibility, and the migration risk for intact-peel fruits is minimal due to the peel barrier and washing or peeling practices, though quantitative migration testing is recommended for future regulatory approval. This work presents a green, waste-to-value strategy aligned with circular economy principles, advancing sustainable and intelligent food packaging systems.

Conclusions

In summary, this study establishes a rational citric acid modulation strategy for the synthesis of customizable CDs from black tea waste, a ubiquitous food processing byproduct. The strategic use of citric acid as a multifunctional modulator was pivotal, delivering a 25.5 fold enhancement in quantum yield and improved photostability, primarily through surface passivation along with controlled core growth. The practical application of these CDs was validated in two distinct, high-impact applications within food systems. First, they were engineered into a robust fluorescent ink, enabling the creation of covert, high-resolution anti-counterfeiting markings on diverse packaging surfaces—entirely invisible under natural light yet exhibiting bright, persistent fluorescence under UV illumination. Second, incorporation into a PVA matrix yielded an active nanocomposite coating that significantly enhanced the post-harvest preservation of strawberries. The composite coating effectively mitigated mass transfer and microbial degradation, as evidenced after 6 days by superior metrics: reduced weight loss, enhanced firmness, and better maintenance of total soluble solids. Our approach provides an effective strategy for upcycling food waste into high value functional materials, thereby advancing the application of CDs in the food industry while supporting green chemistry and a more sustainable food system. Specifically, this work demonstrates the valorization of black tea waste into high value CDs for smart sustainable packaging. The as-prepared CDs exhibit dual functionalities, functioning as covert anti-counterfeiting fluorescent ink and as an active nanocomposite coating for strawberry preservation, which highlights their versatility in intelligent food packaging systems. By employing a green hydrothermal route to valorize a widely available food waste stream, this approach aligns with circular economy principles and offers a sustainable platform for waste derived nanomaterials in the food industry.

Author contributions

Yulu Liu: conceptualization, methodology, investigation, writing-original draft; Jiamin Li: validation, methodology, investigation; Yizhou Xiao: validation, methodology, investigation; Yuchi Chen: validation, methodology, investigation; Yunkai Zhou: validation, methodology, investigation; Fangmei Zhou: writing-review & editing; Bingqi Zhu: writing-review & editing; Wenxiao Jiang: writing-review & editing; Xing Chen: conceptualization, writing-review & editing, validation, funding acquisition; Guangming Li: conceptualization, writing-review & editing, visualization, project administration, funding acquisition.

Conflicts of interest

There are no conflicts to declare.

Data availability

The data supporting this article have been included as part of the supplementary information (SI). Raw data are available from the corresponding author upon reasonable request. Supplementary information is available. See DOI: https://doi.org/10.1039/d6ra03143a.

Acknowledgements

The authors are grateful for the financial support of this study by the National Natural Science Foundation of China (22405245), Jiangxi Double Thousand Plan, China (jxsq2023101077) and the Mindray Joint Fund of Zhejiang Provincial Natural Science Foundation of China (No. LMRY26H200007).

References

1 M. Y. Khalid and Z. U. Arif, *Food Packag. Shelf Life*, 2022, **33**, 100892.
2 Z. Riahi, A. Khan, M. Ebrahimi, J. W. Rhim, G. H. Shin and J. T. Kim, *Compr. Rev. Food Sci. Food Saf.*, 2025, **24**, e70192.
3 H. P. Nguyen, F. Retraint, F. Morain-Nicolier and A. Delahaies, *IEEE Access*, 2019, **7**, 131839–131850.
4 A. Khoshkalampour, M. Ghorbani and Z. Ghasempour, *Food Chem.*, 2023, **404**, 134742.
5 P. Jain, D. Gupta, H. Kaur, S. Singh and K. K. Gaikwad, *Trends Food Sci. Technol.*, 2025, **164**, 105229.
6 X. Xu, R. Ray, Y. Gu, H. J. Ploehn, L. Gearheart, K. Raker and W. A. Scrivens, *J. Am. Chem. Soc.*, 2004, **126**, 12736–12737.
7 Y. L. Hu, O. Seivert, Y. Tang, H. E. Karahan and A. Bianco, *Angew. Chem., Int. Ed.*, 2024, **63**, e202412341.
8 Y. P. Sun, B. Zhou, Y. Lin, W. Wang, K. A. S. Fernando, P. Pathak, M. J. Meziani, B. A. Harruff, X. Wang, H. Wang, P. G. Luo, H. Yang, M. E. Kose, B. Chen, L. M. Veca and S. Y. Xie, *J. Am. Chem. Soc.*, 2006, **128**, 7756–7757.
9 Y. Q. Zhang, Y. Z. Yang, S. R. Ding, X. Zeng, T. Li, Y. S. Hu and S. Y. Lu, *Adv. Mater.*, 2025, **37**, e2418118.
10 S. Y. Lim, W. Shen and Z. Q. Gao, *Chem. Soc. Rev.*, 2015, **44**, 362–381.
11 H. X. Liu, X. Zhong, Q. Pan, Y. Zhang, W. T. Deng, G. Q. Zou, H. S. Hou and X. B. Ji, *Coord. Chem. Rev.*, 2024, **498**, 215468.
12 X. F. Luo, X. Liu, H. D. Guo, R. P. Li, M. Wang, X. T. Li, S. J. Li, S. X. Liu, J. Li, V. Strehmel, Q. Y. Wang, G. Yilmaz, K. Matyjaszewski, B. Strehmel and Z. J. Chen, *Nat. Protoc.*, 2025, **20**, 3695–3721.
13 J. K. Ren, H. Opoku, S. Tang, L. Edman and J. Wang, *Adv. Sci.*, 2024, **11**, 2405472.
14 Y. Wu, Q. Y. Liu, Z. Q. Bu, M. X. Quan, J. Y. Lu and W. T. Huang, *Spectrochim. Acta, Part A*, 2023, **290**, 122291.
15 H. Ren, Z. Miao, J. B. Wang, L. Jin, F. Li and P. Wu, *Biomass Bioenergy*, 2026, **212**, 109293.
16 D. Gupta, R. Priyadarshi, S. K. Tammina, J. W. Rhim and G. Agrawal, *Food Bioprocess Technol.*, 2025, **18**, 2145–2169.

17 C. H. Liu, Y. Q. Mei, Q. W. Lei, X. M. Ma, X. R. Nan, Y. X. Zhu, J. Liao, Y. H. Xu, Y. Luo, H. Q. Zhang, M. Yang, X. F. Lin and Q. T. Huang, *Chem. Eng. J.*, 2024, **499**, 156434.
18 J. Ma, G. X. Huang, J. Li, J. S. Li, L. J. Yan, J. F. Wei and Q. Zhang, *Food Chem.*, 2025, **466**, 142183.
19 Y. Sul, A. Khan and J. W. Rhim, *Food Packag. Shelf Life*, 2024, **43**, 101282.
20 C. Z. Wang, J. W. Yang, X. R. Gu, H. Q. Wang, X. J. Wang, Z. B. Wang and G. Y. Sun, *Food Chem.*, 2025, **472**, 142886.
21 M. Wang, R. Shi, M. J. Gao, K. L. Zhang, L. L. Deng, Q. F. Fu, L. J. Wang and D. Gao, *Food Chem.*, 2020, **318**, 126506.
22 G. Q. Guo, T. T. Li, Z. Y. Liu, X. Y. Luo, T. Zhang, S. Y. Tang, X. Wang and D. Chen, *Food Chem.*, 2024, **432**, 137232.
23 W. Liu, H. P. Diao, H. H. Chang, H. J. Wang, T. T. Li and W. L. Wei, *Sens. Actuators, B*, 2017, **241**, 190–198.
24 T. C. Wareing, P. Gentile and A. N. Phan, *ACS Nano*, 2021, **15**, 15471–15501.
25 P. Duarah, B. Debnath and M. K. Purkait, *Ind. Crops Prod.*, 2024, **221**, 119364.
26 F. Zhao, J. Qian, H. Liu, C. Wang, X. J. Wang, W. X. Wu, D. H. Wang, C. P. Cai and Y. Lin, *Food Chem.*, 2022, **378**, 132130.
27 T. G. Cakmak, B. Saricaoglu, G. Ozkan, M. Tomas and E. Capanoglu, *Food Sci. Nutr.*, 2024, **12**, 3112–3124.
28 S. S. Guo, M. K. Awasthi, Y. F. Wang and P. Xu, *Bioresour. Technol.*, 2021, **338**, 125530.
29 J. H. Wang, Y. F. Wang, J. J. Cheng, J. Wang, X. D. Sun, S. Sun and Z. Y. Zhang, *LWT–Food Sci. Technol.*, 2018, **96**, 90–97.
30 H. Wang, C. Tang, Y. X. Xiang, C. Zou, J. M. Hu, G. P. Yang and W. H. Zhou, *J. Nanobiotechnol.*, 2024, **22**, 146.
31 H. Wang, C. Tang, H. F. Zhang, L. N. Guo, C. Zou, S. T. Zhang, J. L. Liu, Q. P. Huang, Y. J. Liu, W. H. Zhou, G. P. Yang and X. Gao, *J. Controlled Release*, 2025, **388**, 114347.
32 T. Zhao, Z. Z. Chen, X. R. Lin, Z. Y. Ren, B. Li and Y. Y. Zhang, *Carbohydr. Polym.*, 2018, **184**, 164–170.
33 Q. S. He, H. X. Chen, X. Chen, J. J. Zheng, L. F. Que, F. D. Yu, J. H. Zhao, Y. M. Xie, M. L. Huang, C. Z. Lu, J. S. Meng and X. C. Zhang, *Adv. Funct. Mater.*, 2024, **34**, 2310226.
34 Q. L. Ma, Y. F. Yu, M. Sindoro, A. G. Fane, R. Wang and H. Zhang, *Adv. Mater.*, 2017, **29**, 201605361.
35 N. Sharma, S. Thakur, A. Bains, G. Goksen, N. Ali, M. A. Ansari, A. Kopsacheili, C. Proestos and P. Chawla, *Food Chem.: X*, 2025, **25**, 102043.
36 W. A. Ye, S. Yang, R. T. Jin, D. Liang, Z. Y. Ren and R. Lin, *Food Biosci.*, 2025, **65**, 106037.
37 Y. He, S. Q. Liu, F. Xie, Y. Zhou, X. S. Yang and J. Food, *Compos. Anal.*, 2024, **132**, 106332.
38 A. Khan, P. Ezati and J. W. Rhim, *Food Packag. Shelf Life*, 2023, **37**, 101075.
39 Qurtulen and A. Ahmad, *Environ. Sci. Pollut. Res.*, 2023, **30**, 121630–121646.
40 L. Zhang, Z. L. Cai, Y. Q. Liu, Y. Fan and Y. B. She, *Front. Sustain. Food Syst.*, 2024, **8**, 1431792.
41 A. Konwar, N. Gogoi, G. Majumdar and D. Chowdhury, *Carbohydr. Polym.*, 2015, **115**, 238–245.
42 A. Konwar, U. Baruah, M. J. Deka, A. A. Hussain, S. R. Haque, A. R. Pal and D. Chowdhury, *ACS Sustainable Chem. Eng.*, 2017, **5**, 11645–11651.
43 M. Z. Qu, H. J. Yu, Y. C. He, W. D. Xu, D. Liu and F. Cheng, *Chem. Eng. J.*, 2024, **486**, 150266.
44 Y. Kim, K. L. Goodner, J. D. Park, J. Choi and S. T. Talcott, *Food Chem.*, 2011, **129**, 1331–1342.
45 H. Unyay, H. O. Altay, N. A. Perendeci, S. Szufa, F. Ozdemir and I. Angelidaki, *J. Environ. Chem. Eng.*, 2025, **13**, 117124.
46 B. H. Li, Y. Wang, J. C. Zhang, Y. B. Li, B. Li, Q. L. Lin, R. J. Sun, F. J. Fan, Z. P. Zeng, H. B. Shen and B. T. Ji, *Nat. Commun.*, 2025, **16**, 2450.
47 A. Zoha, M. Ejaz, F. Nawaz, M. A. Mohsin, M. N. Zafar and Z. Ali, *RSC Adv.*, 2026, **16**, 21584–21590.
48 H. Ding, S. B. Yu, J. S. Wei and H. M. Xiong, *ACS Nano*, 2016, **10**, 484–491.